Computers and Geotechnics 159 (2023) 105464

Contents lists available at ScienceDirect

Computers and Geotechnics

journal homepage: www.elsevier.com/locate/compgeo

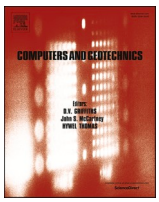

Installation performance of structurally enhanced caissons in sand

Moura Mehravar [a,*], Ouahid Harireche [b], Asaad Faramarzi [c], Farough Rahimzadeh [c], Ashraf Osman [d], Samir Dirar [c]

[a] College of Engineering and Physical Science, Aston University, Birmingham, the United Kingdom of Great Britain and Northern Ireland
[b] Islamic University of Madinah, Faculty of Engineering, Department of Civil Engineering, Saudi Arabia
[c] School of Engineering, University of Birmingham, Edgbaston, Birmingham, the United Kingdom of Great Britain and Northern Ireland
[d] Deparment of Engineering, Durham University, the United Kingdom of Great Britain and Northern Ireland

ARTICLE INFO

Keywords:
Flanged suction caissons
Installation feasibility in sand
Soil resistance
Finite element modelling
Piping condition
Numerical framework

ABSTRACT

Suction caissons are attractive solutions to support offshore structures. Their capacity, both pull-out and bearing, grows with their embedment depth. However, higher embedment depths increase risks of installation failure due to uncertainty of seabed condition, increased chance of piping and structural buckling. For the first time, this paper investigates installation of structurally enhanced caissons (SECs), in the form of flanges attached to the caisson shaft, through developing a numerical procedure based on finite element analysis. The *SEC* has the potential to offer additional (over 20%) pull-out and bearing capacity compared with standard caisson and can have substantial positive impacts on torsional capacity. Using the proposed numerical procedure, the impact of adding the flanges on the installation resistance was studied and compared against a standard caisson. A piping criterion was defined which allows tracking the soil region where piping develops and evolves as the installation proceeds. The impacts of flange base sizes and sand compaction on the required suction for installation were studied. The results of this paper can be used as guidance to predict the required suction to install flanged caissons and can facilitate the uptake of the proposed *SEC*. The proposed numerical framework is applicable to other *SEC* geometries.

1. Introduction

A suction caisson is an upturned thin walled 'bucket' of cylindrical shape made from steel. This type of foundation has proven to be efficient and versatile as a support for offshore oil and gas structures and appears to be a very attractive foundation for supporting offshore wind turbines (Byrne, et al., 2002; Byrne and Houlsby, 2003; Zhao, et al., 2018). Compared to pile foundations, caisson foundations offer several advantages; for instance, they are more cost effective, easy to install and can be easily removed at the end of their service life (Byrne, et al., 2002; Byrne and Houlsby, 2003; Houlsby, et al., 2005; Faramarzi, et al., 2016; Kim, et al., 2017; Bienen, et al., 2017; Le, et al., 2018; Harireche, et al., 2021).

In general, foundations for offshore wind turbines (OWTs), including caissons, are subjected to various loadings comprising vertical, horizontal, and moment loads or combinations of all of these. In particular, they experience large overturning moments due to the significant horizontal wind pressures acting high above the foundation level (Gourvenec and Jensen, 2009; Vilalobos, et al., 2004; Faizi, et al., 2019; Mehravar, et al., 2016). Lateral loads or moments are more critical for wind turbine foundations compared to vertical loads (Kim, et al., 2016a). The resistance of these foundations to overturning moments, is the biggest challenge facing designers (Zhu, et al., 2014). Due to the increase in demand for generating energy from renewable sources, there is a need to enhance the capacity of caisson foundations of offshore wind turbines (OWTs) either when the overturning capacity is not sufficient to withstand the overturning moment or when additional overturning capacity is needed, e.g., to support hyper tall wind turbines (>100 m). Moreover, caisson foundations are subjected to a high magnitude of pull-out loading when they are employed as anchors for floating offshore wind turbines. Increasing caisson dimensions (i.e., diameter and/or embedment depth) is often the primary method of improving the foundation bearing capacity. However, apart from imposing additional costs, increasing the depth, grows the risks of potential structural buckling during installation, as well as the failure of installation due to uncertainties associated with seabed geotechnics.

* Corresponding author.
E-mail address: m.mehravar@aston.ac.uk (M. Mehravar).

https://doi.org/10.1016/j.compgeo.2023.105464
Received 10 April 2022; Received in revised form 4 April 2023; Accepted 5 April 2023
Available online 21 April 2023
0266-352X/© 2023 The Authors. Published by Elsevier Ltd. This is an open access article under the CC BY license (http://creativecommons.org/licenses/by/4.0/).

To address the above challenges and to improve the static and dynamic performance of OWT caisson foundations, a series of novel systems of skirted/caisson foundations have been presented in recent years (Dimmock, et al., 2013; Fu, et al., 2014; Kim, et al., 2016b; Zhang, et al., 2016; Wang, et al., 2018). Typical enhanced foundations consist of a combination of a standard caisson with another type of foundation (Gaudin, et al., 2011; Choo, et al., 2016) or include additional structural elements (Davidson, et al., 2018; Fu, et al., 2014) with the aim of improving the foundation bearing capacity or stiffness and reducing its rotation and/or settlement. While these works have indicated possible design solutions to improve the in-service performance of various caisson foundations, their applications and uptakes are hampered by difficulties encountered during construction or installation. The majority of the proposed hybrid foundations have complex structures and are unproportionally large and heavy. Manufacturing, transportation, and installing such foundations can be costly and require complicated machinery. A novel, yet practical, design of caisson foundations would be beneficial to tackle issues linked to the bearing or pull-out capacities whilst addressing challenges associated with their logistics.

Only limited studies have been conducted to investigate the installation performance of novel caissons. Zhang, et al. (2017) and Zhang, et al. (2018) explored the installation performance of a novel caisson design which consists of a bucket foundation with a bulkhead. The authors performed laboratory experiments and numerical simulations and investigated the impact of seepage on changes in soil resistance that occur during installation. In their numerical modelling, they used a steady-state finite element analysis to study seepage during installation under different seabed conditions. Katarzyna Koteras and Ibsen (2021) investigated a modular bucket foundation design for large offshore wind turbines that consisted of trapezoidal profiles bolted together and additional stiffeners attached at the inner side of the skirt. They performed both jacking and suction installation tests on large-scale models of their new proposed design as well as standard circular shaped caissons. They concluded that despite the increase in soil resistance of the modular foundation, the required suction for installation was similar for both models. A number of other studies looked at centrifuge and numerical modelling of so-called stiffened caissons in clay, where ring stiffeners are typically added to inside the caisson structure to increase its stiffness and improve performance against buckling during installation (Zhou et al., 2016; Zhou et al., 2022; Wang et al., 2021; Wang et al., 2020). Generally, the contribution of stiffeners to improve the capacity of anchors is ignored as they are considered to be negligible. Given the complexity and challenges associated with the uncertainty of offshore projects, finding novel, yet practical ways of increasing the capability of OWT caisson foundations to carry large horizontal, overturning, and pull-out loads while minimising the installation resistance and ensuring efficiency and sustainability, is vital. At the same time, while most design efforts are concentrated on developing caisson foundations with various fit-for-purpose specifications, it is evident that any newly developed design must consider the impact on the installation process.

This paper explores the potential use of a structurally enhanced caisson (*SEC*) that consists of a set of vertical triangular flanges annexed to the exterior surface of a standard circular caisson by investigating the impact of the flanges on the installation procedure. The proposed *SEC* has the potential to extend lateral, pull-out and overturning capacities of standard caissons without adding complexity to the foundation design. Additionally, previous studies have shown that caissons with flanges have the potential to demonstrate superior torsional capacity (Darby, et al., 2019).

For the first time, this paper focuses on the installation process of *SEC* in sand, where the impact of suction induced seepage is critical to a successful installation. The main aim of this paper is to investigate the impacts of the additional structural elements (i.e. the flanges) on the installation resistances using a novel numerical framework. This novel framework is based on a finite element numerical procedure used to predict the magnitude of penetration resisting forces taking into account the suction-induced seepage. To this end, the analytical formulations derived by Harireche, et al. (2021) to predict the frictional and tip resistance of a standard caisson are extended to include the resisting forces of the flanges and are implemented in COMSOL Multiphysics. The magnitude of soil resistance is then used to estimate the required suction magnitude at different penetration depths. Problem dimensions are normalised so that the results obtained are independent of *SEC* prototype and can be applied to any *SEC* size. The impact of soil loosening inside the caisson cavity is also included in the numerical model. Based on the developed numerical model, critical conditions for piping during the whole installation process are tracked. Firstly, the numerical model is validated based on the simulation of a couple of field tests reported by Houlsby and Byrne (2005). In the next step, the proposed numerical model is employed to investigate the impact of the flange base size on the installation performance of SECs. Model prediction of the required suction at different stages of installation and the critical condition for piping are highlighted for the proposed SECs. Finally, the installation performance of a *SEC* is explored in various sand properties. The proposed numerical framework can be employed and extended to predict the required amount of suction for installation of various flanged caisson (different number of flanges, shapes etc.).

2. *SEC* installation in homogenous sand

2.1. Introduction

In general, a suction assisted installation relies on a precise prediction of soil resistance and critical soil conditions which may occur during the installation procedure (Harireche, et al., 2021). The thin caisson wall facilitates installation under a pressure differential induced by suction, and when the seabed profile consists of sand layers, seepage reduces the soil resistance against caisson penetration. This is achieved as a result of reducing the effective stress, which in turn reduces the mobilised frictional resistance that develops around the embedded caisson wall (Senpere and Auvergne, 1982; Tjelta, et al., 1986; Erbrich and Tjelta, 1999; Tran, et al., 2004; Tran, et al., 2005; Chen, et al., 2016; Mehravar, et al., 2017; Harireche, et al., 2021). Cone Penetration Tests (CPTs) performed by Senders and Randolph (2009) revealed a significant sand loosening inside the caisson cavity during the installation of suction caissons. While seepage is advantageous to caisson installation in sand and granular deposits, suction magnitude must be controlled to ensure a safe installation and avoid critical soil conditions such as piping (Bye, et al., 1995; Tjelta, 1994; Tjelta, 1995; Ibsen and Thilsted, 2010; Ibsen and Thilsted, 2011; Harireche, et al., 2021). The effects of suction induced seepage on soil-skirt interaction and penetration resistance have also been investigated by centrifuge model tests (Allersma, 2003; Tran and Randolph, 2007; Tran and Randolph, 2008), laboratory experiments (Bang, et al., 1999; Villalobos, 2006; Lian, et al., 2014), and finite element simulations (Vasquez and Tassoulas, 2000). In the following sections, model's geometry, development and validations are presented, followed by analyses of the proposed *SEC* design.

2.2. SEC geometry

The shape of the structurally enhanced caisson (*SEC*) proposed in this study consists of a standard caisson with three triangular flanges attached vertically to the main shaft, at 120°angle intervals (Fig. 1a). Alongside the *SEC* and for reference, a standard suction caisson is considered as shown (Fig. 1b).

The standard caisson consists of a cylinder of wall thickness t_c, and inner and outer radii R_i and R_o, respectively. The flanges extend over the height of the caisson and have same thickness (t_f) as the caisson wall ($t_c = t_f$). Fig. 2 shows the geometrical properties of *SEC* and illustrates the coordinates system r, ξ used in this study. The internal diameter of the caisson is denoted as D and the investigated flange base, b_f, varies from $0.15D$ to $0.25D$.

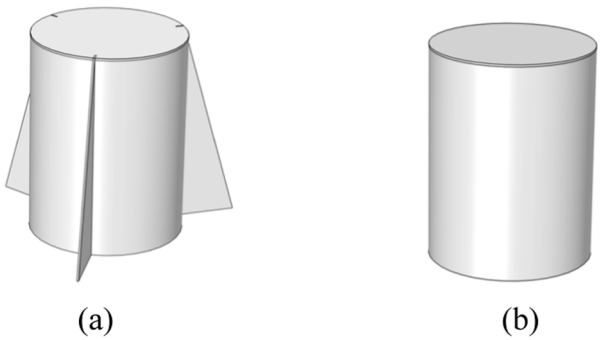

Fig. 1. (a) Schematic 3D drawing of a *SEC*, (b) Standard caisson.

For simplicity, the installation is assumed to take place in homogenous sand with permeability k and saturated unit weight γ_{sat}. However, sand loosening inside the caisson cavity, due to the upward seepage, is considered as it may cause a local increase in soil permeability.

2.3. Formulation of the resisting forces against the SEC penetration

During the installation of a standard caisson, in addition to tip resistance, a frictional resistance develops on both inner and outer wall surfaces. It's important to accurately predict these resistance modes, particularly in the case of suction-induced seepage assisted installation (Harireche, et al., 2021). In *SEC*, some additional resistance develops due to the existence of the three flanges. This consists of friction and tip resistances that develop on each flange (Fig. 3). In Fig. 3, h denotes the penetration depth at a time t during the installation procedure. In order to draw conclusions that are not affected by the prototype dimensions, all dimensions and porewater pressures have been normalised with respect to the caisson inner radius (R_i) and the suction magnitude ($\bar{s}$).

In this study, we adopt the following normalisation procedure of the main problem variables and we denote:

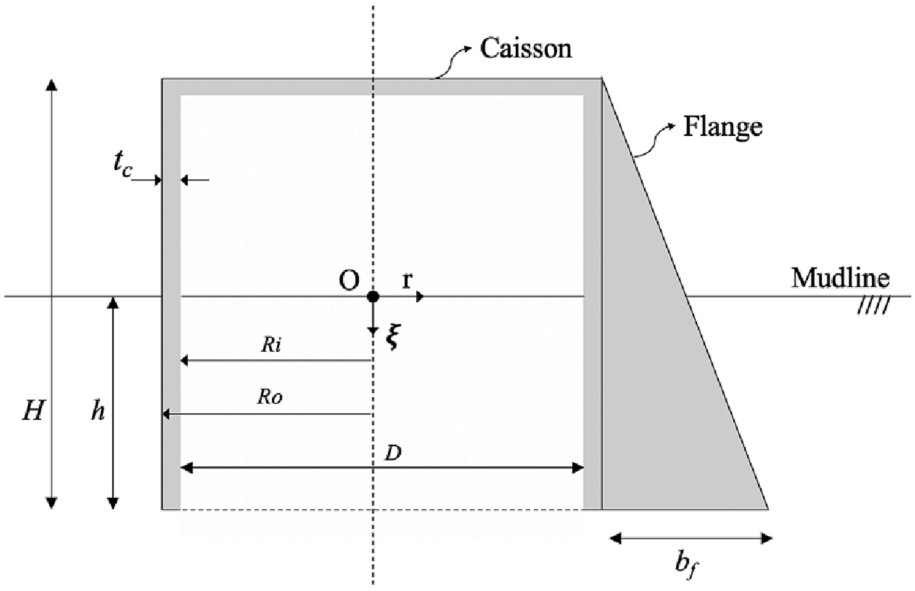

Fig. 2. Geometry of a *SEC*.

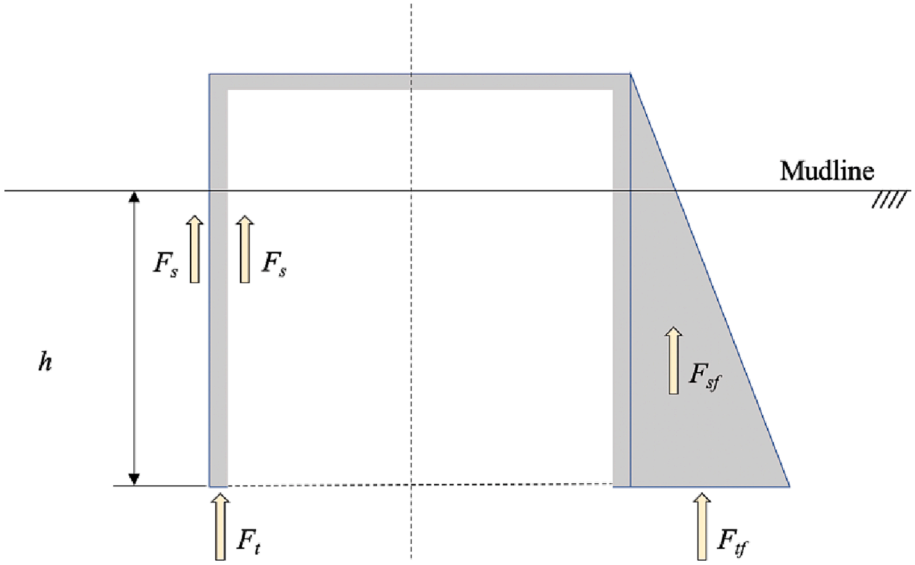

Fig. 3. Resisting forces against *SEC* penetration.

$$p^* = \frac{p}{\bar{s}} \tag{1}$$

the dimensionless counterpart of the excess porewater pressure,

$$h^* = \frac{h}{R}, \xi^* = \frac{\xi}{R}, r^* = \frac{r}{R}, b_f{}^* = \frac{b_f}{R} (0 \le r^* \le 1) \tag{2}$$

the dimensionless counterparts of the caisson penetration depth, the vertical and radial coordinates, and the flange base. Assuming three flanges, the total resisting force F_T can be expressed as:

$$F_T = F_s + F_t + 3(F_{sf} + F_{tf}) \tag{3}$$

where F_s and F_t are forces resulting from frictional and tip resistances, respectively. These forces are expressed on the normalised geometry as follows:

$$F_s = \pi K \tan\delta \left[(fR_i + R_o)\gamma' h^{*2} R^2 - 2\bar{s}R(fR_i I_i^* + R_o I_o^*) \right]$$

$$I_i^* = \int_0^{h^*} (p_i^* + 1) d_\xi^* I_o^* = \int_0^{h^*} p_o^* d_\xi^* \tag{4}$$

$$F_t = \pi R N_q t_c \left[2\gamma' h - \bar{s}(p_{ih}^* + p_{oh}^* + 1) \right] + \pi R N_\gamma \gamma' t_c{}^2 \tag{5}$$

Parameter K in Equation (4) is the coefficient of lateral soil pressure, $tan\delta$ is the coefficient of friction at the soil-caisson interface. The coefficient f represents sand loosening under upward seepage inside the caisson cavity ($f \ll 1$) (Harireche, et al., 2014).

In this study, the magnitude of coefficient f has been estimated using a few trials within the seepage simulation using COMSOL Multiphysics. Such effect has been studied in details by Harireche, et al., (2014).

Normalised excess porewater pressures induced by suction on the inner and outer sides of the caisson wall are denoted as $p_i{}^*$ and $p_o{}^*$, respectively and γ' denotes the soil buoyant unit weight. In Equation (5), parameters N_q and N_γ are bearing capacity factors at the foundation tip, related to surcharge and soil self-weight (Houlsby, et al., 2005), p_{ih}^* and p_{oh}^* denote excess pore pressures on the inner and outer wall sides, respectively.

In each flange, wall friction and tip resistance result in forces F_{sf} and F_{tf} expressed by:

$$F_{sf} = R^2 K tan\delta \left[R\gamma' b^* b^{*2} \left(1 - \frac{h^*}{3H^*} \right) - 2\bar{s} I_f{}^* \right] \tag{6}$$

where

$$I_f{}^* = \int_A p_o^*(r^*, \xi^*) d_r{}^* . d_\xi{}^*$$

$$F_{tf} = N_q . t_f{}^* \left[\gamma' R^3 h^* b^* - \bar{s} R^2 I_{tf}^* \right] + \frac{1}{2} N_\gamma t_f{}^{*2} . \gamma' R^3 b_f{}^{*2} \tag{7}$$

where $I_{tf}^* = \int_1^{1+b_f^*} p_{oh}^* d_r{}^*$.

It should be noted that the expressions of frictional forces in Equations (4) and (6) were derived from a Coulomb criterion applied to the interfaces between the soil and the *SEC* walls and flanges. Consequently, the suction required to achieve a caisson penetration depth h can be expressed by:

$$S = \frac{F_{s+} F_t + 3(F_{sf} + F_{tf})}{\pi R_i^2} \tag{8}$$

More details on the derivation of the above formulations are given in appendix A and for a standard caisson can be found in (Harireche, et al., 2021).

2.4. Validation approach

In the present work, two set of experimental data reported by Houlsby and Byrne (2005) and obtained from the field trials at Tenby (field trial 1) and Sandy Haven (field trial 2) were employed to validate the developed numerical procedure for a standard caisson.

In both field trials the seabed formation consists of dense sand with a unit weight of 18.3 kN/m^3, a friction angle of 40° and an estimated factor $K \times \tan\delta$ of 0.48 (Houlsby and Byrne, 2005). In Tenby trial, the installation experiment was performed using a standard caisson prototype which had a diameter of 2 m, a height of 2 m and a wall thickness of 8 mm, while the caisson employed in Sandy haven trial had a diameter of 4 m, height of 2.5 m and a wall thickness of 20 mm.

3. A numerical model for *SEC* installation

The installation performance of caisson and *SEC* is analysed to obtain the required suction profile based on the force required to overcome soil resistance (8). To this aim, the numerical procedure presented in Section 2.3 was implemented in COMSOL Multiphysics. Per each installation depth (h^*) a normalised suction pressure ($p^* = \frac{p}{\bar{s}} = -1$) is prescribed at the mudline level (Fig. 4). The model investigates the porewater seepage within the soil volume around the embedded part of the foundation wall and flanges. This model is used to estimate soil resistance, given the importance of seepage in the mitigation of lateral soil pressure and hence, the reduction of mobilised friction on caisson walls and flanges.

3.1. Governing equations

Prior to the caisson installation, water pressure is in hydrostatic condition with an ambient absolute magnitude at depth ξ, $p_0 = p_{at} + \gamma_w h_w + \gamma_w \xi$, where p_{at} is the atmospheric pressure, γ_w the unit weight of water and h_w the water height above mudline. A deviation of the porewater pressure from the hydrostatic value at any location within the soil is referred to as excess porewater pressure. After caisson penetration (both standard caisson and *SEC*) under self-weight, a total penetration depth h is reached under a prescribed suction of constant magnitude $\bar{s}$ at the mudline level, inside the caisson cavity. It is important to note that suction has a negative value; however, the magnitude $\bar{s}$ is a positive number. Upon prescribing the suction ($\bar{s}$) a negative excess porewater pressure is generated in the soil and around the foundation. Within the soil mass, the porewater seepage is assumed to obey Darcy's law. Hence, the velocity field within the soil mass is determined by the gradient of excess porewater pressure, p, dynamic water viscosity, μ [Pa.s] and intrinsic soil permeability, κ [m^2], as follows:

$$u = \frac{\kappa}{\mu} (\nabla p) \tag{9}$$

3.2. Boundary conditions and model geometry

In addition to the equation governing Darcy's velocity field, u and excess porewater pressure, p, appropriate boundary conditions must be specified. Fig. 4 shows the prescribed boundary conditions in a normalised geometry. On the mudline, at the outer side of the caisson wall, and on the lateral far boundaries, the excess porewater pressure is zero. On the far bottom boundary, the flow normal to the boundary is zero ($\boldsymbol{u}.\boldsymbol{n} = 0$) where $\boldsymbol{n}$ is the outward unit normal vector to the boundary. Moreover, normal flow to the embedded parts of the caisson, including the caisson wall and flanges, is zero ($\boldsymbol{u}.\boldsymbol{n} = 0$).

Taking advantage of the symmetrical nature of the problem, only half of the entire system is simulated in a three-dimensional FE model (Fig. 5 (a-b)). Fig. 5 (a) shows a semi-cylindrical section through a radial plane of a *SEC* ($b_f{}^* = 0.25$ D $= 0.5$R). This figure also represents the typical finite element mesh of the foundation, used in this study. A number of different mesh densities in which element sizes around the

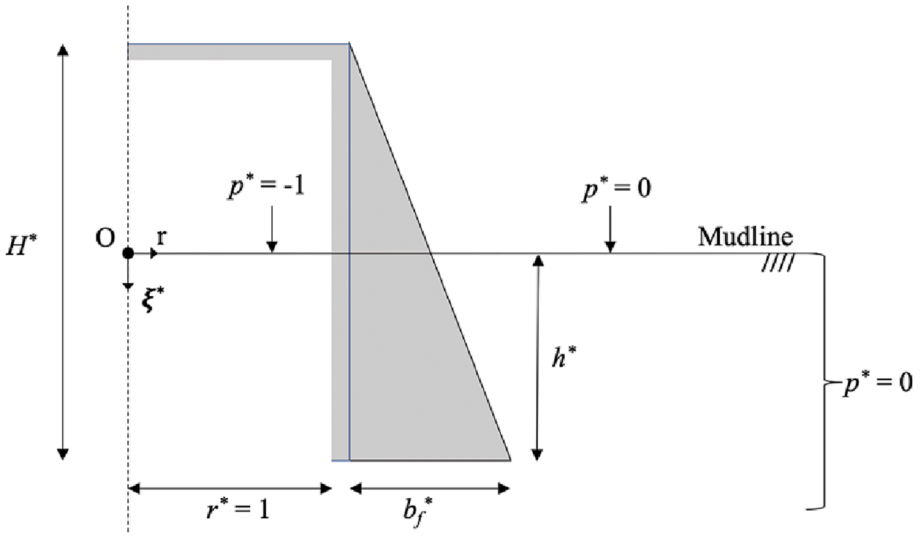

Fig. 4. Boundary conditions.

caisson wall and tip are considerably refined were tested to obtain convergent results in a reasonable computational time. The mesh is extended 6R from the centre line of the caisson foundation, so that the results are not sensitive to the boundary conditions. The FE simulations were single-phase fluid (using porous media and subsurface flow module of COMSOL Multiphysics). In the FE models presented in this paper, soil effective stresses around the caisson wall as well as flanges, were calculated indirectly using the changes in porewater pressure. To this aim, the derived formulations in section 2.3 were implemented in COMSOL-Multiphysics and soil effective forces at various stage of installation were computed. In other words, by applying $p^*= -1$ in COMSOL Multiphysics model described above, the excess porewater pressure generated in the soil and around the foundation can be measured (p_i^*, p_o^*). Then, the derived formulations (4–8) are implemented in COMSOL Multiphysics, and used to calculate the effective forces generated around the foundation at various stage of the installation. Finally, using Equation 8, required value of suction for the installation at different penetration depth can be predicted. The x-y plane view of a *SEC* is shown in Fig. 5 (b), where the flanges and caisson are highlighted in red.

3.3. Numerical results

3.3.1. Preliminary numerical results and model validation

The numerical framework described in this study is now applied to model the installation process of two suction assisted installation of the standard caisson prototypes used in Tenby and Sandy Haven field trials (Houlsby and Byrne, 2005) as described in section 2.4.

The data recorded from both field trials, which consist of suction magnitude at different penetration depths, together with the simulation results are shown in Figs. 6a-b.

Fig. 6a shows that the numerical predictions do not match the field trial measurements if the effect of soil loosening inside the caisson cavity is not included. This is the case where f in Equation (4) is given a value of 1. It is important to note that the discrepancy between experimental data and predicted results increases with the normalised depth, suggesting that, not only f should be smaller than unity, but it must also increase as installation progresses in order to reflect continuous soil loosening as suction increases. Indeed, further testing with values of f smaller than unity but constant during the installation process led to the same conclusion. Therefore, the coefficient f must be varied throughout the installation and must be a function of the normalised penetration depth of h^*. The following simple linear expression which was proposed by Harireche et al. (2014), is employed here:

$$f(h^*) = \alpha h^* \tag{10}$$

After some trials with the simulation of seepage of a standard caisson based on the trial caisson installed in Tenby, value of the parameter α was identified as 0.015. With this value, the numerical model was calibrated, and the simulation results match very well with those of the field data (Figs. 6a-b). This comparison with experimental data highlights the importance of soil loosening inside the caisson cavity as a result of suction induced seepage during the whole installation process. Expression (10) provides a simple description of the parameter f to quantitively reflect such loosening effects. While this validation exercise highlights the suitability of the simple assumed form of the parameter f in Equation (10), further experiments are required to justify whether the parameter α is constant or dependent on other parameters. In addition, Figs. 6a-b illustrate the ability and accuracy of the proposed numerical framework to predict the suction magnitude for suction assisted caisson installation as well as the accuracy of the proposed formula for the parameter f.

3.3.2. Critical suction for piping condition

In sand, upward seepage inside the caisson cavity develops a seepage force acting against gravity, which may cause a critical soil condition where the effective vertical stress becomes zero. Such a condition is known as piping. A criterion for piping is expressed by:

$$\frac{\partial p}{\partial z} = \gamma' \tag{11}$$

Developing piping channels during caisson installation is critical since it will cause damage to the seal between the soil and the caisson wall and ultimately will lead to installation failure. Critical suction for piping has been investigated in different studies (Houlsby and Byrne, 2005; Ibsen and Thilsted, 2011; Harireche, et al., 2013; Harireche, et al., 2014; Wu, et al., 2017; Alluqmani, et al., 2019; Harireche, et al., 2021). At early penetration stages, piping is limited to the caisson tip but will extend upwards to a larger region inside the caisson cavity as the installation proceeds. To determine the region subjected to piping inside the caisson cavity, the following condition is employed (Harireche, et al., 2021):

$$\mu \geqslant 1 \tag{12}$$

where function μ is defined by $\mu(r^*, z^*) = \frac{1}{\gamma'}\frac{\partial p}{\partial z} = \frac{\bar{s}}{\gamma' R} g_i^*(r^*, z^*)$ and $g_i^*(r^*, z^*)$ is the normalised gradient of excess porewater pressure at the inner side

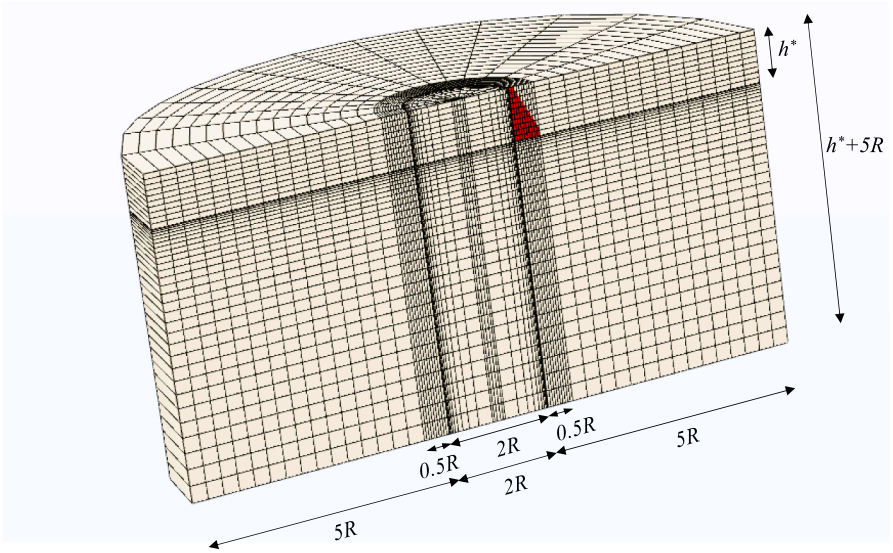

(a)

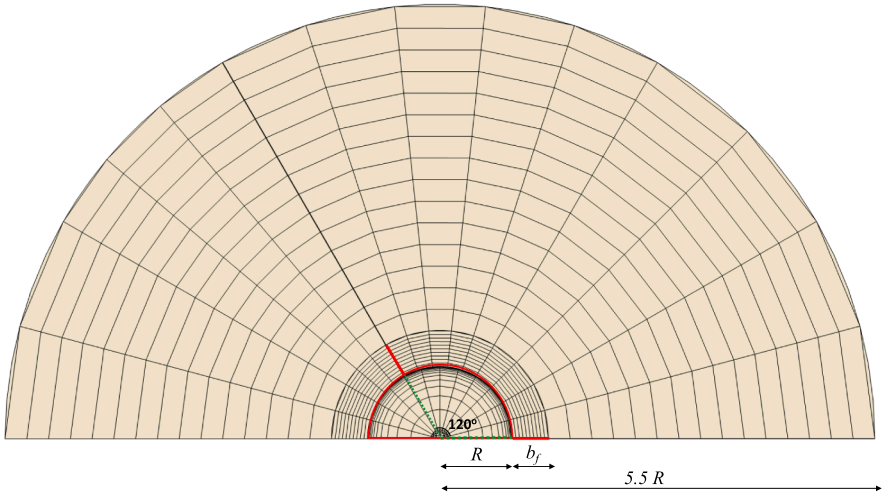

(b)

Fig. 5. (a) Finite element mesh; (b) x-y plane view of a *SEC* model (not to scale).

of the caisson wall. This criterion was implemented into COMSOL Multiphysics to investigate the piping domain as the standard caisson installation proceeds (Tenby field trial). In the finite element simulations of the installation process, the soil region where piping develops and evolves as the installation proceeds, can be tracked based on the criterion (12). Fig. 7 (a-c) show contours of function μ for the field trial at Tenby at different penetration depths of 0.5 m, 1 m, and 1.4 m. In this figure the isolines corresponding to the μ equal to unity are shown by black bold line.

The contour with a value equal to unity corresponds to the boundary of the region affected by piping. It can be seen from Fig. 7 (a-c) that by increasing the installation depth, larger volume of sand within the caisson cavity is affected by piping. Fig. 7 (a) illustrates that at an early stage of caisson penetration, when h^*=0.5, the piping condition is limited mainly to the lower half of the penetration depth, and piping channel has not been fully developed yet. As the installation proceeds, and when h^*=1 (Fig. 7 (b)), the piping zone propagates, and about half of the soil mass inside the caisson cavity is subjected to piping. Additionally, Fig. 7 (c) shows that once the installation depth reaches to 1.4 m, a depth that showed a loss of suction in the field trial at Tenby (Houlsby and Byrne, 2005), majority of the soil inside the caisson cavity is affected by the piping condition. These numerical results and observations related to the development and propagation of piping during the installation confirm the reliability and accuracy of the numerical model developed in this study. It is worth noting that an increasing pumping rate during the installation process may accelerate the formation of piping channels in critical conditions (Harireche et al., 2021). However, this effect has not been included in the present model for conciseness of the numerical procedure, which is devoted here primarily to the aspects related to the added structural flanges.

3.3.3. *SEC installation: modelling and results*

It is instructive to apply the described and validated numerical framework to predict the installation resistances of the *SEC* and explore the impact of the added flanges on the installation performance compared to a standard caisson. To this aim, different SECs (Fig. 1(a)) where the size of the attached flanges are different, were numerically modelled, and their results were compared against a standard caisson.

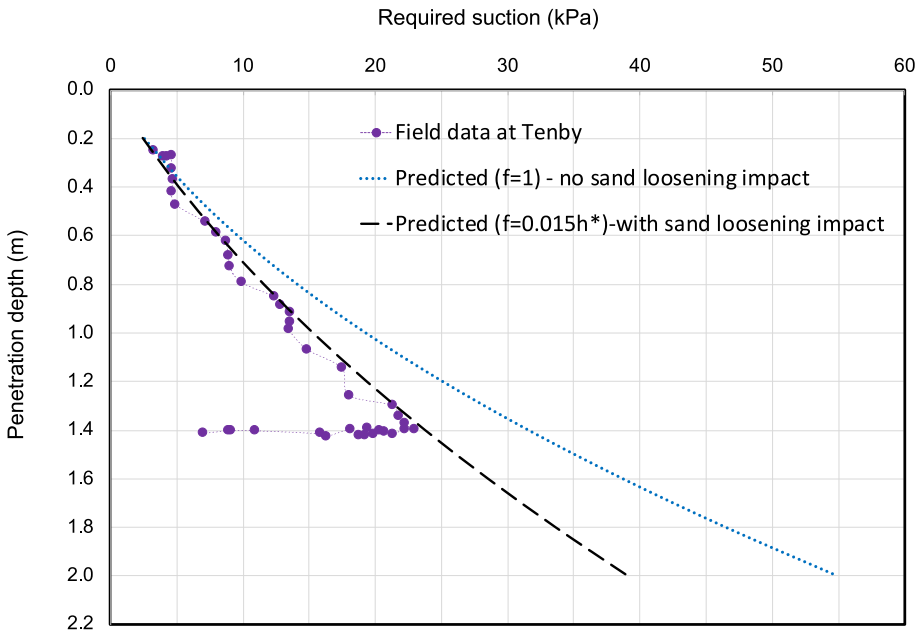

Fig. 6a. Validation of numerical model against field data at Tenby.

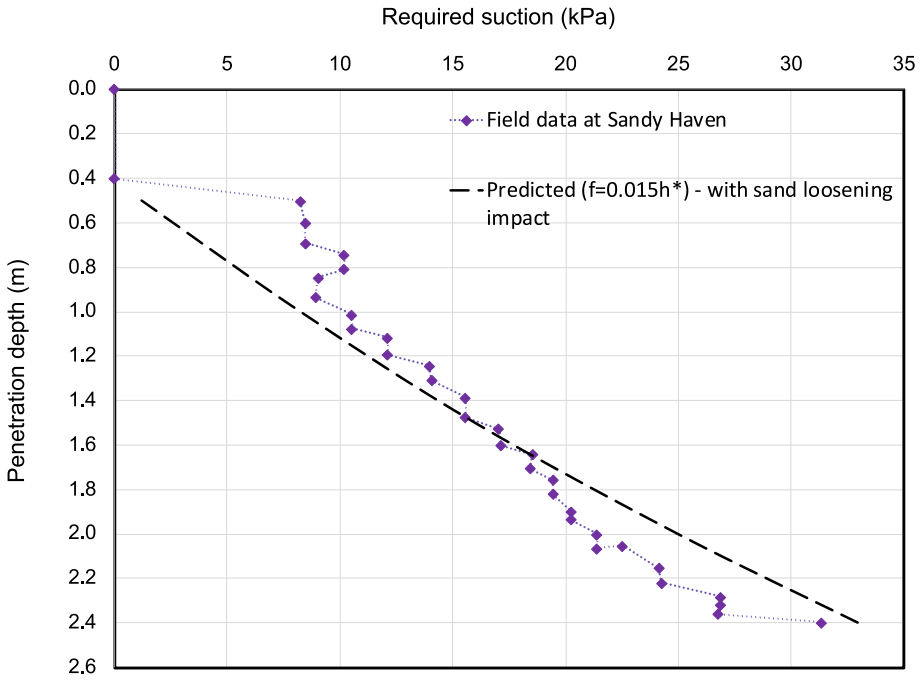

Fig. 6b. Validation of numerical model against field data at Sandy Haven.

Details of the SECs and the standard caisson are presented in Table 1. The models are assumed to be installed in a typical European offshore site where the ground condition can be approximated by a sand with buoyant unit weight of $\gamma' = 9.7kN/m^3$ and an angle of shearing resistance of 30° (Bhattacharya, et al., 2009); (Kuhn, 2001).

The predicted suction profiles required to install the SECs models (presented in Table 1) are shown in Fig. 8. Additionally, the suction required to install a standard caisson (caisson model I in Table 1), is presented for comparison. In Fig. 8, both penetration depth and suction magnitude are presented in terms of their normalised values; the magnitude of the required suction was normalised by $\gamma' D$ with respect to the soil where γ' is the buoyant unit weight of soil and D is the caisson diameter. Compared to a standard caisson, the SECs require a higher amount of suction for installation. The difference between the required suction for the installation of SECs and the standard caisson increases with the installation process. The numerical results indicate that the magnitude of suction required to fully install a *SEC* to a standard depth, $h^* = 2$, with a flange base size of 0.15*D*, 0.2*D* and 0.25*D*, will increase by about 18 %, 25 % and 30 %, respectively, compared to the standard caisson.

As discussed in section 3.3.2, piping develops at the inner side of the caisson and evolves as the installation proceeds and the suction increases. To get more insight into the suction assisted installation of the *SEC* (caisson model II and model IV), piping zones at different stages of the installation were investigated using the function μ. The contours were obtained for four different penetration depths of $h^* = 0.5, 1, 1.5, 2$

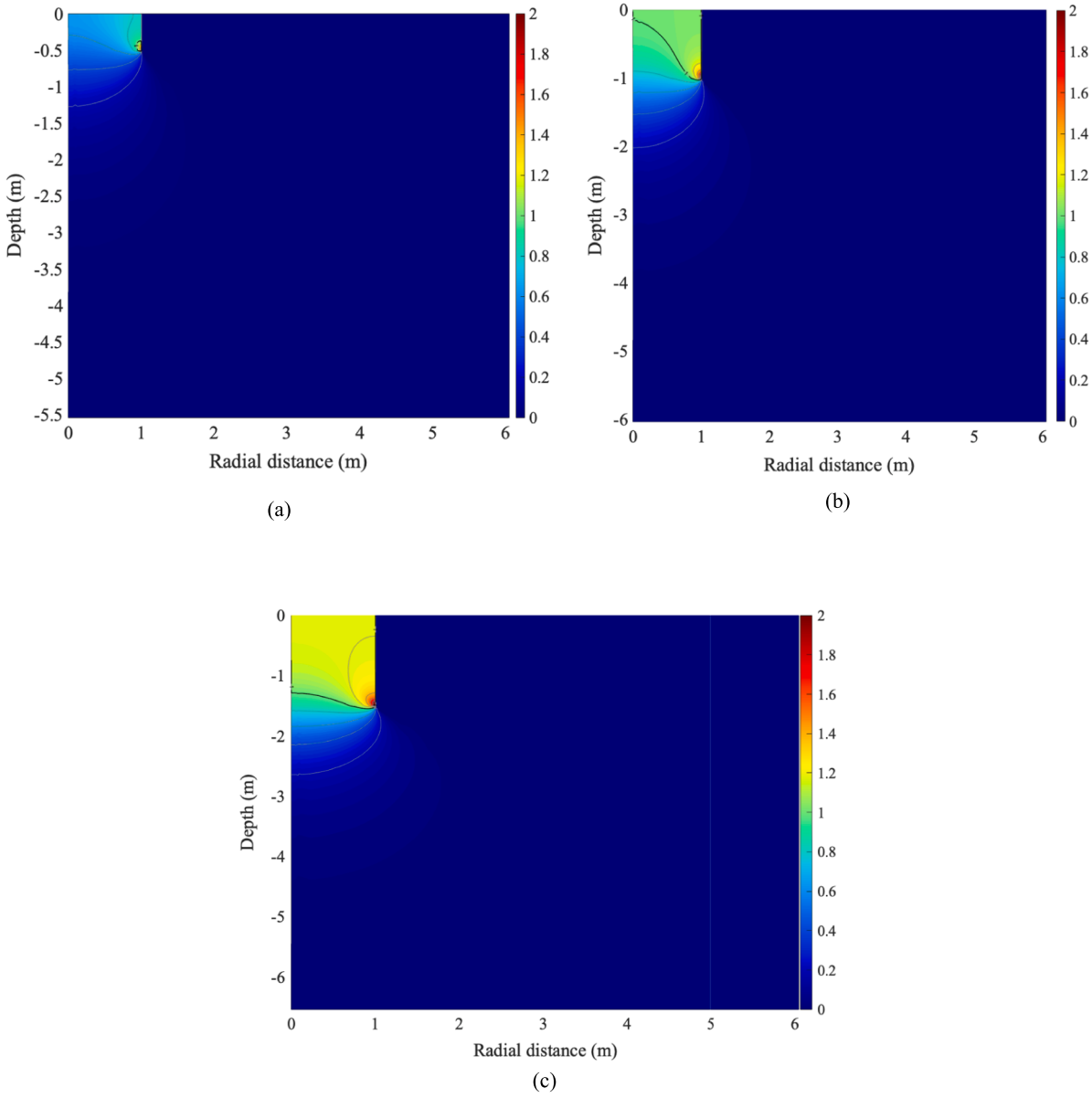

Fig. 7. (a-c). Predicted contours of function μ for the Tenby field trial.

to explore at which stage of the installation a significant volume of soil inside the caisson cavity is subjected to piping. As expected, at an early stage of the installation (h^*=0.5 and 1), piping is localised at the caisson tip for both flange base sizes – see Fig. 9 (a-b)-10(a-b), while for h^*=1.5 and 2, piping condition extends over the whole penetration depth, which may lead to a loss of suction, Fig. 9(c-d) and 10 (c-d). However, this piping channel can be avoided by reducing the pumping rate for a slower but safer installation. It should be noted that in this study, suction has been imposed directly on the mudline and the pumping rate is not controlled in the simulation. However, the piping criterion represented by the function μ offers useful information that helps limiting the pumping rate for a safe and successful installation.

3.4. Parametric study

Caisson model IV (Table 1) was selected and its installation performance in different soil conditions from very loose to dense sand, was investigated. To this aim, four different seabed formations with different friction angles ranging from 27° to 36°, buoyant unit weight of 9.7 kN/m^3 and a factor $K \times \tan(\delta)$ of 0.48 (Houlsby and Byrne, 2005) were considered. These values of the soil angle of friction are selected to cover seabed formations ranging from very loose sand to dense sand (Peck, et al., 1974) (Table 2).

In general, the results of the parametric study (Fig. 11) provide useful evidence on how the required suction at different stages of the installation of a *SEC* changes with the angle of internal friction of the soil. It also offers an insightful information for future development of a criterion to describe in which sandy seabed the installation of the proposed SECs is feasible. This information is particularly important as the increase in required suction due to the added flanges, is more pronounced for soils with high frictional strength.

The results which are presented as normalised values both for required suction and penetration depth (see section 3.3.3) indicate that by increasing the soil friction angle, the required amount of suction increases, even at early stages of the installation process ($h^* \geq 0.5$). This increasing trend is nonlinear and the nonlinearity becomes more noticeable at larger penetration depths– for example, within the second half of the installation depth, when $h^* \geq 1$ and $\phi \geq 33$. At this stage, it can be observed that, to fully penetrate a *SEC* with flange base size of

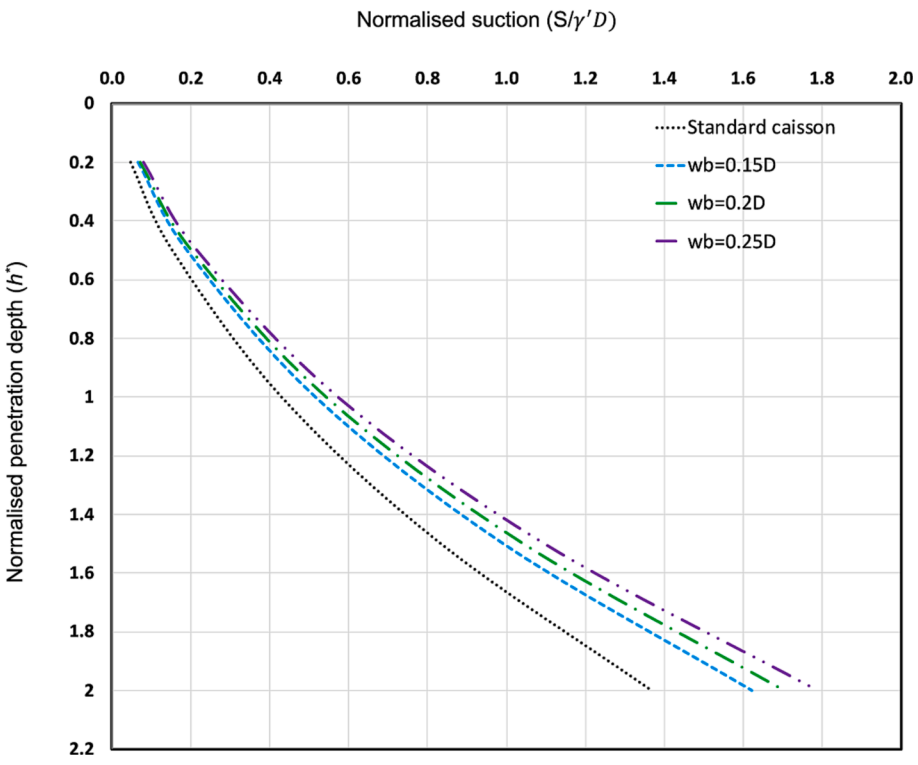

Fig. 8. Impact of flange base size on the required suction for installation in sand ($\gamma' = 9.7kN/m^3$ and $\phi = 30^{\circ}$).

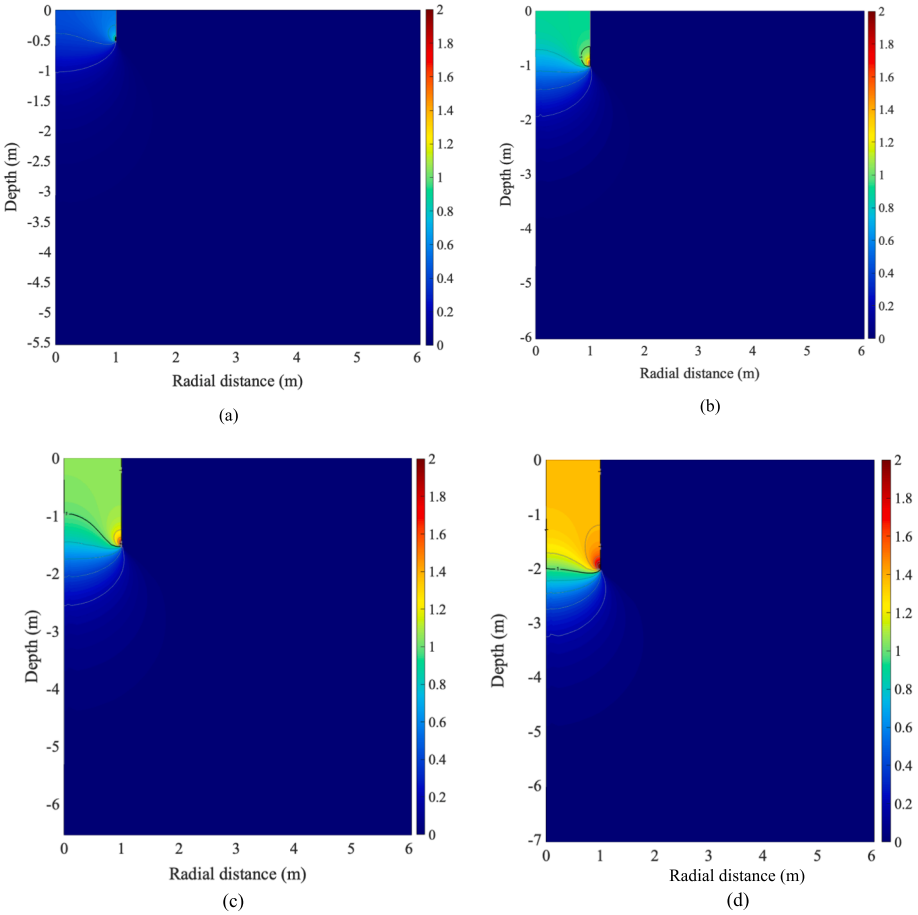

Fig. 9. Contours of function μ in a flanged caisson with a flange base size of 0.15D, at different depths (a) h^*=0.5, (b) h^* =1, (c) h^*=1.5 and (d) h^*=2, installed in sand ($\gamma' = 9.7kN/m^3$ and $\phi = 30^{\circ}$.

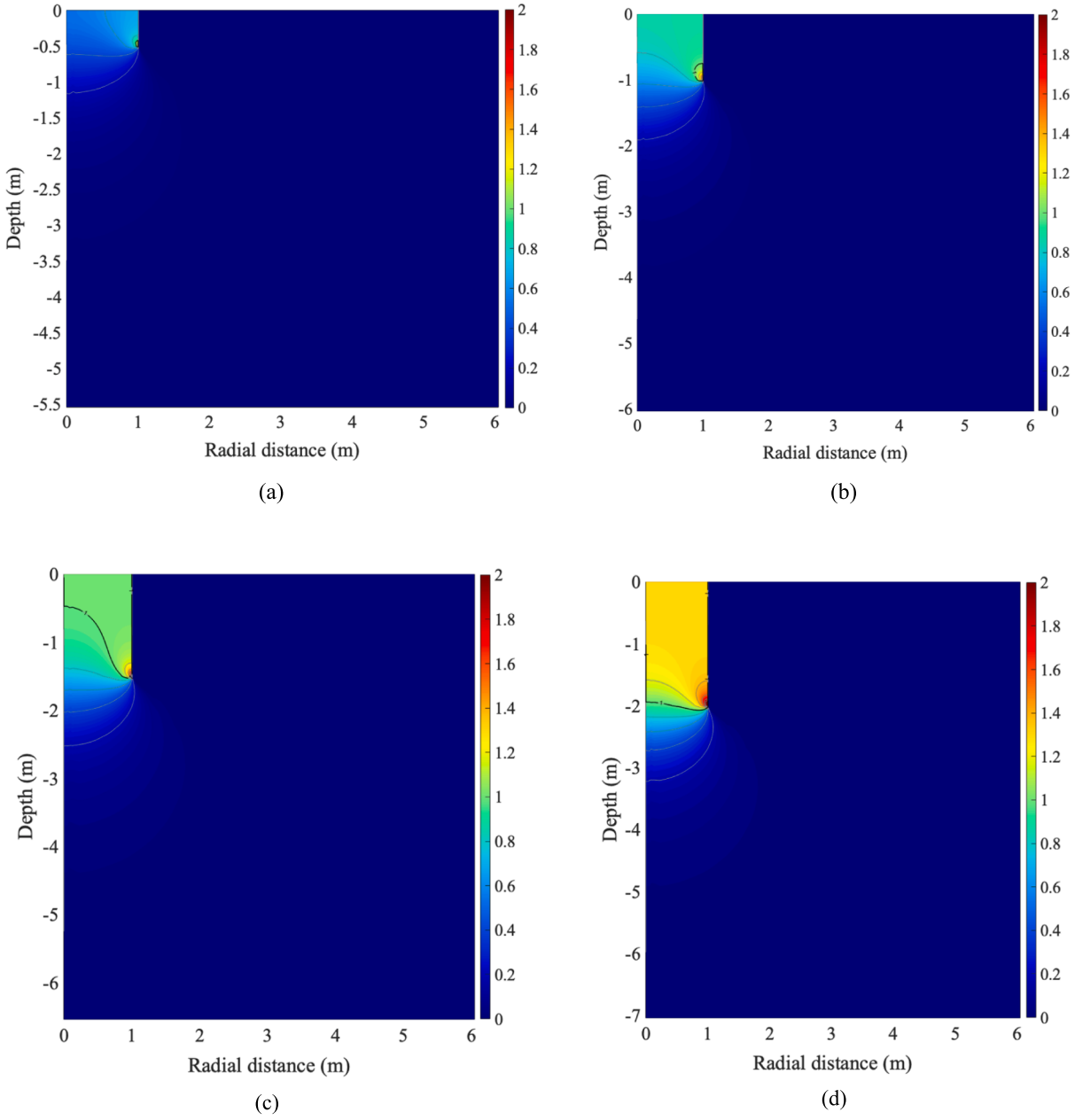

Fig. 10. Contours of function μ in flanged caisson with flange base size of 0.25D, at different depths (a) h^*=0.5, (b) h^* =1, (c) h^*=1.5 and (d) h^*=2, installed in sand ($\gamma' = 9.7kN/m^3$ and $\phi = 30^\circ$).

0.25*D* (caisson model IV) in very dense sand ($\phi = 39^\circ$), the applied suction should be increased by about 70 % compared to the case where the installation takes place in loose sand ($\phi = 27^\circ$).

4. Summary and conclusions

This study has been motivated by the need for a novel offshore caisson foundation that potentially can increase pull-out resistance and overturning bearing capacity compared to the standard caisson. The focus was mainly on the feasibility and safety of the installation process. To this aim, the installation of a structurally enhanced caisson (*SEC*) foundation was investigated in various sands. The *SEC* considered in this study consists of a standard caisson with three triangular flanges perpendicularly attached to the outer wall at 120°intervals. Three different sizes of flanges were studies in this paper. A numerical procedure of the normalised model problem was firstly developed based on porewater seepage around the *SEC* walls, described by Darcy's model. Normalised pressure gradient was used to investigate soil resistance to the *SEC* penetration and critical conditions for piping. The full numerical procedure was implemented in COMSOL Multiphysics to predict the required amount of suction at different stages of installation. The numerical model was validated using a simulation of two real field trials taking into account the sand loosing within the caisson cavity. The effect of the flanges and their base size on the installation resistance was also discussed. A piping criterion was defined to identify the regions subjected to piping inside the caisson cavity at different stages of the *SEC* installation. Critical piping was first analysed for a standard caisson and its prediction confirmed the installation difficulties faced during Tenby's field trial. A parametric study was conducted to investigate the impact of soil condition (soil internal friction angle) on the penetration resistance during the whole installation process of the SECs.

The results of this study quantified the additional soil resistance and

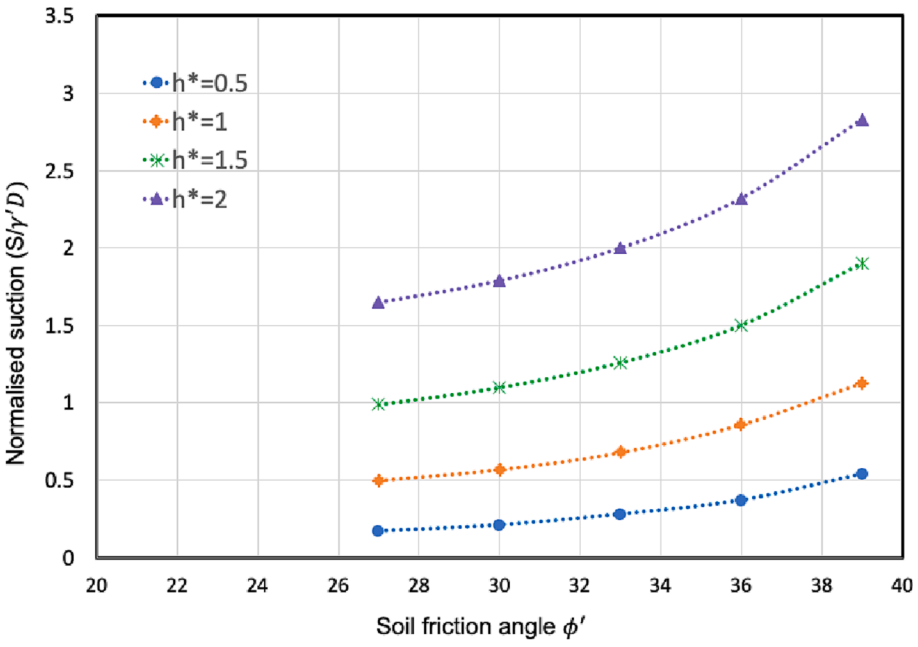

Fig. 11. Normalised suction required to install the flanged caisson IV in different sands.

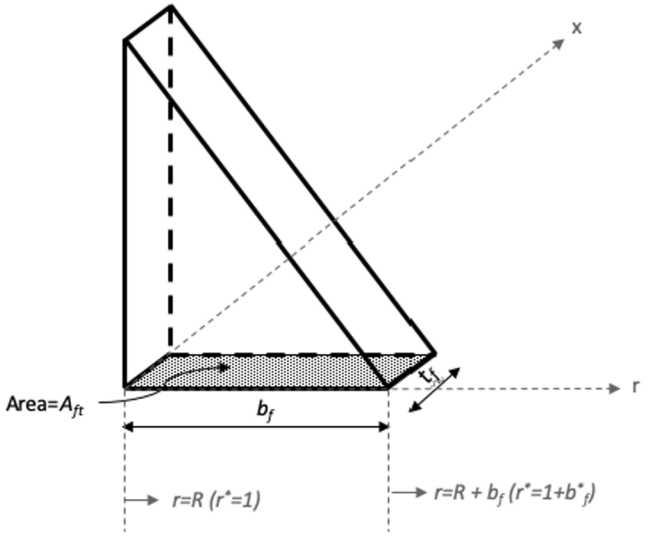

Fig. A1. Schematic three-dimensional geometry of a flange.

Table 1
Dimensions of different enhanced caisson models.

Caisson model	Diameter (D): m	Length (L): m	Thickness (t): mm	Flange shape	Wing base length (b): m
I	2	2	8	No flange	0 D (standard caisson)
II	2	2	8	Triangular	0.15D
III	2	2	8	Triangular	0.2D
IV	2	2	8	Triangular	0.25D

hence the additional suction required to install SECs with different flange base sizes relative to the case of a standard caisson. The magnitude of additional soil resistance depends on the flange base size. It was observed that, compared to a standard caisson, an *SEC* with a flange base size of 0.15*D*, 0.2*D* and 0.25*D*, will require an increase of suction magnitude about 18 %, 25 % and 30 %, respectively, at full installation depth.

Table 2
Different soil internal friction angles used in the parametric study.

Soil ID	Soil type	ϕ': deg
A	Very loose sand	27
B	Loose sand	30
C	Medium dense sand I	33
D	Medium dense sand II	36
E	Dense sand	39

The results of the parametric study show how soil resistance against caisson installation increases nonlinearly with an increasing friction angle. For instance, compared to an installation in loose sand ($\phi = 27^{\circ}$), the full installation of an *SEC* with a flange base of 0.25D in denser sands with friction angles 30°, 33°, 36°, and 39°, requires an increase in suction by 8.5 %, 13 %, 19 % and 31 %, respectively. The developed numerical procedure for suction prediction of the SECs can be easily extended and applied for different flange's geometries (e.g., rectangular and trapezium) as well as different flange numbers.

CRediT authorship contribution statement

Moura Mehravar: Conceptualization, Methodology, Software, Validation, Formal analysis, Visualization, Investigation, Supervision, Writing – original draft, Writing – review & editing, Funding acquisition. **Ouahid Harireche:** Methodology, Investigation, Formal analysis, Validation, Writing – review & editing. **Asaad Faramarzi:** Conceptualization, Methodology, Formal analysis, Writing – review & editing. **Farough Rahimzadeh:** Software, Investigation, Visualization. **Ashraf Osman:** Validation, Writing – review & editing. **Samir Dirar:** Writing – review & editing.

Declaration of Competing Interest

The authors declare that they have no known competing financial interests or personal relationships that could have appeared to influence the work reported in this paper.

Data availability

No data was used for the research described in the article.

Acknowledgement

The first author would like to thank the Supergen Offshore Renewable Energy (ORE) hub for supporting this project.

Appendix A

Total pressure at depth ζ below the mudline (P_ζ) in presence of applied suction is:

$$P_\xi = \gamma_w (h_w + \xi) + p_\xi \tag{A1}$$

where p_ξ is excess pore pressure produced by suction-induced seepage. Under seepage conditions produced by an applied suction, excess porewater pressure at depth inside and outside the caisson wall is repressively expressed as follows:

$$p_i(\xi) = -\bar{s} + \int_0^\xi g_i(\xi) d_\xi \tag{A2}$$

$$p_o(\xi) = \int_0^\xi g_o(\xi) d_\xi \tag{A3}$$

where $\bar{s}$ is a magnitude of applied suction, p_i and p_o is pressure inside and outside of the caisson wall, respectively, g_i and g_o denote the vertical component of the pressure gradient on the inner and outer side of the caisson respectively and can be expressed as follows:

$$g_i = \frac{\partial p_i}{\partial \xi} > 0, \quad g_o = \frac{\partial p_o}{\partial \xi} < 0 \tag{A4}$$

It is important to note that suction has a negative value; however, the magnitude s is a positive number. In this paper, we consider the excess porewater pressure gradient in terms of the magnitude of its vertical component at each location within the soil mass. This is motivated by the fact that such component defines the seepage force that acts against gravity and directly affects effective stresses.

On the inner side of caisson wall, the effective stress changes/reduces by $\int_0^\xi g_i(\xi) d_\xi$ compared to its magnitude, $\gamma' \xi$, in hydrostatic condition (A5).

$$\sigma_{vi}(\xi) = \gamma' \xi - \int_0^\zeta g_i(\xi) d_\xi = \gamma' \xi - (p_i(\xi) + \bar{s} \tag{A5}$$

On the outer side, the effective stress is expressed by:

$$\sigma_{vo}(\xi) = \gamma' \xi - \int_0^\xi g_o(\xi) d_\xi = \gamma' \xi - p_o(\xi) \tag{A6}$$

The net reduction in effective stress at depth ξ is given by:

$$\Delta\sigma'_v = \int_0^\xi g_i(\xi) d_\xi + \int_0^\xi g_o(\xi) d_\xi \tag{A7}$$

On the other hand, numerical simulations on the normalised geometry of the suction caissons shows that $\int_0^\xi g_i(\xi) d_\xi > \left| \int_0^\xi g_o(\xi) d_\xi \right|$. This means $\Delta\sigma'_v > 0$, which is the advantage of a controlled suction installation.

Mobilised frictional resistance $\tau_i(\xi)$ and $\tau_o(\xi)$, on the inner and outer sides of the caisson wall respectively, are given by:

$$\tau_i(\xi) = (K.tan\delta)\sigma' v_i(\xi) \tag{A8}$$

$$\tau_o(\xi) = (K.tan\delta)\sigma' v_0(\xi) \tag{A9}$$

where K is a coefficient of lateral soil pressure and $tan\delta$ is the coefficient of friction at the soil-caisson interface.

The lateral frictional force acting on caisson wall can be written under the following form:

$$F_s = \int_0^h 2\pi R_i \tau_i d_\xi + \int_0^h 2\pi R_o \tau_o d_\xi \tag{A10}$$

where $\int_0^h 2\pi R_i \tau_i d_\xi$ and $\int_0^h 2\pi R_o \tau_o d_\xi$ denote to frictional force acting inside and outside the caisson wall, respectively and can be rewritten as:

$$\int_0^h 2\pi R_i \tau_i d_\xi = 2\pi R_i \int_0^h f K \tan\delta \, \sigma'_{vi} d_\xi = 2\pi R_i f K \tan\delta \int_0^h \sigma'_{vi} d_\xi \tag{A11}$$

$$\int_0^h 2\pi R_o \tau_o d_\xi = 2\pi R_o \int_0^h f K \tan\delta \, \sigma'_{vo} d_\xi = 2\pi R_o K \tan\delta \int_0^h \sigma'_{vo} d_\xi \tag{A12}$$

and by substituting (A5) and (A6) into (A11) and (A12) respectively, the lateral force acting on both sides on the caisson can be calculated as follows:

$$R_i f\,\beta \int_0^h \sigma_{vi}^{'} d_\xi = R_i\,\beta f \int_0^h (\gamma^{'}\,\xi - (p_i\,(\xi) + \bar{s}))\,d_\xi = R_i f\,\beta \left[\gamma^{'}\frac{h^2}{2} - \int_0^h (p_i + \bar{s}) d_\xi)\right] \tag{A13}$$

$$R_o\,\beta \int_0^h \sigma_{vo}^{'} d_\xi = R_o\,\beta \int_0^h (\gamma^{'}\,\xi - p_o)\,d_\xi = R_o\,\beta \left[\gamma^{'}\frac{h^2}{2} - \int_0^h p_o d_\xi\right] \tag{A14}$$

where β is defined by $2\pi K\tan\delta$ and consequently total lateral force on caisson wall can be expressed as:

$$F_s = \pi\,K\tan\delta\left[(fR_i + R_o)\gamma^{'}h^2 - 2fR_i\int_0^h (p_i + \bar{s}) d_\xi - 2R_0\int_0^h p_0 d_\xi\right] \tag{A15}$$

The resisting force at the caisson tip can be expressed under the form (Houlsby and Byrne, 2005):

$$F_t = N_q \int_{A_t} \sigma_t^{'}\,d_A + \frac{1}{2}\,\gamma^{'}\,t\,N_\gamma\,A_t \tag{A16}$$

where N_q and N_γ are bearing capacity factors, t is caisson wall thickness, A_t is base area at the caisson tip and $\sigma_t^{'}$ is vertical effective stress at caisson tip. Given the small thickness of caisson where $\frac{R_o - R_i}{R_i} \ll 1$ then the vertical effective stress at the caisson tip at penetration depth of h can be described by:

$$\sigma_t^{'} \approx \frac{1}{2}\left(\sigma_{vi}^{'}(h) + \sigma_{vo}^{'}(h)\right) = \gamma^{'}h - \frac{1}{2}\,(\bar{s} + p_{ih} + p_{oh}) \tag{A17}$$

where $\sigma_{vi}^{'}(h)$ and $\sigma_{vo}^{'}(h)$ are vertical effective stress at depth h at the caisson tip inside and outside, respectively. In this equation also p_{ih} and p_{oh} are excess porewater pressure magnitude at depth of h (at the caisson tip) inside and outside, respectively. Consequently, by substituting (A16) into (A17) resisting force at caisson tip can be expressed as:

$$F_t = \pi\,R\,N_q[2\,\gamma^{'}h - (p_{ih} + p_{oh} + \bar{s}] + \pi\,R\,N_q\gamma^{'}\,t^2 \tag{A18}$$

In order to draw conclusions that are not affected by the prototype dimensions, we adopt the following normalisation procedure of the main problem variables and we denote:

$$p^{*} = \frac{p}{\bar{s}} \tag{A19}$$

The dimensionless counterpart of the excess porewater pressure and

$$h^{*} = \frac{h}{R}\,,\; z^{*} = \frac{z}{R},\; r^{*} = \frac{r}{R}\;(0 \le r^{*} \le 1)\;\text{on OC and}\;1 \le r^{*} \le \infty\;\text{on CF} \tag{A20}$$

Using the normalised depth (z^{*}) as well as normalised excess porewater pressure (p^{*}), equation 15 and 16 can be expressed as follows:

$$F_s = \frac{\beta}{2}\left[(fR_i + R_o)\gamma^{'}h^2 - 2\bar{s}R(f\,R_i\,I_i^{*} + R_o\,I_o^{*})\right] \tag{A21}$$

where $I_i^{*} = \int_0^{h^{*}} (p_i^{*} + 1) d_\xi^{*}$ and $I_o^{*} = \int_0^{h^{*}} p_o^{*} d_\xi^{*}$

$$F_t = \pi\,R\,N_q\left[2\,\gamma^{'}h - \bar{s}\,(p_{ih}^{*} + p_{oh}^{*} + 1\right] + \pi\,R\,N_q\gamma^{'}\,t^2 \tag{A22}$$

The added flanges will increase the installation resistance and its magnitude depends on the base size of the flanges. Frictional resistance on both sides of the flange (See Fig. 4) can be expressed as:

$$F_{sf} = 2K\,tan\delta \int_A \sigma_v^{'}\,d_A \tag{A23}$$

where effective vertical stress at different locations on the caisson flanges can be described by:

$$\sigma_v^{'}(r,\xi) = \gamma^{'}\,\xi - \int_0^\xi g_o(r,\xi) d_\xi = \gamma^{'}\,\xi - p_o(r,\xi) \tag{A24}$$

and

$$\int_A \gamma^{'}\,\xi\,d_A = \frac{bh^2\,\gamma^{'}}{2}\,(1 - \frac{h}{3H}) \tag{A25}$$

Therefore on the normalised geometry where $p^{*} = \frac{p_o}{\bar{s}}, d_r^{*} = \frac{d_r}{R}\; and d_\xi^{*} = \frac{d_\xi}{R}$ the frictional force acting on different places of the caisson wall is given by:

$$F_{sf} = R^2 K\,tan\delta\left[R\gamma^{'}\,b_f{}^{*}\,h^{*\,2}\left(1 - \frac{h^{*}}{3H^{*}}\right) - 2\bar{s}\,I_f^{*}\right] \tag{A26}$$

where

$$I_f^* = \int_{A^*} p^*(r^*, \xi^*)\, d_r^*\, d_\xi^* \tag{A27}$$

To obtain the required amount of suction which is required to penetrate the enhanced caisson into the soil, tip resistance on the wing should be estimated. Fig. 1A shows a schematic three-dimensional geometry of a wing with base length and thickness of b and t_f, respectively. The thickness of the wings is considered to be similar to the thickness of the caisson ($t = t_f$).

Tip resistance on a flange (F_{tf}) is given by:

$$F_{tf} = N_q \int_{A_{ft}} \sigma_t' dA + \frac{1}{2}\gamma' t_f N_\gamma A_{ft} \tag{A28}$$

where effective stress at different radial distances of the wall at penetration depth of h is described as:

$$\sigma_t'(r) = \gamma' h - p_{oh}(r) \tag{A29}$$

where p_{oh} is excess porewater pressure at penetration depth h on the outer side of the caisson which its variation over the radial distance from the caisson wall can be expressed as:

$$\int_{A_{ft}} p_{oh}(r)\, dA = \int_R^{R+b_f} p_{oh}(r)\, t_f\, d_r = \int_1^{1+b_f^*} \bar{s}\, p_{oh}^*(r^*)\, R^2\, t_f^*\, d_r^* \tag{A30}$$

After developing (A28) and substitution of (A29) and (A30), on normalised geometry tip resistance at a wing tip can be expressed by:

$$F_{tf} = N_q\, t_f^* \left[\gamma' R^3 h^*\, b_f^* - \bar{s} R^2 I_{tf}^*\right] + \frac{1}{2} N_\gamma\, t_f^{*2}\, \gamma' R^3 b_f^* \tag{A31}$$

where

$$I_{tf}^* = \int_1^{1+b_f^*} p_{oh}^*\, d_r^* \tag{A32}$$

References

Allersma, H.G.B., 2003. Centrifuge research on suction piles: installation and bearing capacity. Design and Practice.

Alluqmani, A.E., Naqash, M.T., Harireche, O., 2019. A standard formulation for the installation of suction caissons in sand. J. Ocean. Eng. Sci. 4, 395–405.

Bang, S., Cho, Y., Preber, T., Thomason, J., 1999. Model testing and calibration of suction pile installation in sand. Seoul, South Korea, In: 11th Asian Regional Conference on Soil Mechanics and Geotechnical Engineering.

Bhattacharya, S., Carrington, T. & Aldri, T., 2009. Observed increases in offshore pile driving resistance. *Proceedings of the Institution of Civil Engineers - Geotechnical Engineering* , 162 1 pp. 71-80.

Bienen, B., O'Loughlin, C. D. & Zhu, F. Y., 2017. *Physical modelling of suction bucket installation and response under long-term cyclic loading.* s.l., In: Proceedings of 8th Offshore Site Investigation and Geotechnics International Conference (OSIG 2017) .

Bye, A., Erbrich, C. T., Rognlien, B. & Tjelta, T. I., 1995. *Geotechnical design of bucket foundations.* Houston, Texas, Paper OTC 7793, In: Offshore Technology Conference.

Byrne, B.W., Houlsby, G.T., 2003. Foundations for offshore wind turbines. Philos. Trans. R. Soc. Lond. A 361, 2909–2930.

Byrne, B.W., Houlsby, G.T., Martin, C., Fish, P., 2002. Suction caisson foundations for offshore wind turbines. Wind Eng. 26 (3), 145–155.

Chen, F., et al., 2016. Large scsle experimental investigation of the installation of suction caisssons in silt sand. Appl. Ocean Res. 60, 109–120.

Choo, Y.W., et al., 2016. Numerical studies on piled gravity base foundation fro offshore wind turbine. Mar. Georesour. Geotechnol. 34, 729–740.

Darby, L., et al., 2019. Finite element modelling of winged suction caissons in clay under uniaxial and combined loading. s.l., In 2nd International Conference on Natural Hazards and Infrastructure.

Davidson, C., et al., 2018. Centrifuge modelling of screw piles for offshore wind energy foundations. s.l., 9th International Conference on Physical Modelling in Geotechnics.

Dimmock, P., et al., 2013. Hybrid subsea foundaations for subsea eqiupment. J. Geotechn. Geoennviron. Eng. 139, 2128–2192.

Erbrich, C. T. & Tjelta, T. I., 1999. *Installation of bucket foundations and suction caissons in sand: geotechnical performance.* Houston, Texas, Paper OTC 10990, In: Offshore Technology Conference (OTC).

Faizi, K., Faramarzi, A., Dirar, S., Chapman, D., 2019. Monotonic and cyclic lateral load tests on monopod winged caisson foundations in sand. Institution of civil Eng. – Geotechn. Eng. 173 (5), 448–460.

Faramarzi, A., Faizi, K., Dirar, S., Mehravar, M. and Harireche, O., 2016. Modelling the seepage flow during caisson installation in a natural seabed.

Fu, D., Bienen, B., Gaudin, C., Cassidy, M., 2014. Undrained capacity of a hybrid subsea skirted mat with caissons under combined loading. Can. Geotech. J. 51, 934–949.

Gaudin, C., et al., 2011. Centrifuge experiments of a hybrid foundation under combined loading. s.l., The twenty-first International Offshore and Polar Engineering Conference.

Gourvenec, S., Jensen, K., 2009. Effect of embedment and spacing of cojoined skirted foundation system on undrained limit states under general loading. Int. J. Geomech. 9, 267–279.

Harireche, O., Mehravar, M., Alani, A.M., 2013. Suction caisson installation in sand with isotropic permeability varying with depth. Appl. Ocean Res. 43, 256–263.

Harireche, O., Mehravar, M., Alani, A.M., 2014. Soil conditions and bounds to suction during the installation of caisson foundations in sand. Ocean Eng. 88, 163–173.

Harireche, O., Naqash, M.T., Farooq, Q.U., 2021. A full numerical model for the installation analysis of suction caissons in sand. Ocean Eng. 234, 1–14.

Houlsby, G. T. & Byrne, B. W., 2005. Design procedures for installation of suction caissons in sand. *Proceedings of the Institution of Civil Engineers, Geotechnical Engineering* , 158(3), pp. 135-144.

Houlsby, G. T., Ibsen, L. & Byrne, B. W., 2005. *Suction caissons for wind turbines.* Perth, Australia , In Frontiers in Offshore Geotechnics. ISFOG.

Ibsen L.B. Thilsted C.L. 2010 Numerical study of piping limits for installation of large diameter buckets in layered sand 2010 Trondheim, Norway. In: Proceedings of the Seventh European Conference on Numerical Methods in Geotechnical Engineering.

Ibsen, L. B. & Thilsted, C. L., 2011. Numerical study of piping limits for suction installation of offshore skirted foundations and anchors in layered sand. *Frontiers in Offshore Geotechnics II - Gourvenec & White* , Volume ISBN: 978-0-415-58480-7.

Katarzyna Koteras, A., Ibsen, L.B., 2021. Installation of novel suction bucket foundation with new modular geometry in a large-scale set-up. J. Waterw. Port Coast. Ocean Eng. 147 (4), 04021011.

Kim, J.H., et al., 2016b. Bearing capacity of hybrid suction foundation on sand with loading direction via centrifuge model test. Japanese Geotechn. Soc. Spacial Publications 2, 1339–1342.

Kim, Y., Ahn, J., Jung, J., 2017. Fuzzy modelling of holding capacity of offshore suction caisson anchors. Int. J. Numer. Anal. Methods GeoMech 41, 1038–1054.

Kim, D., Choo, Y.W., Park, J.H., Kwak, K., 2016a. Review of offshore monopile design for wind turbine towers. Japanese Geotechn. Soc. Special Publication 4, 158–162.

Kuhn, M., 2001. Dynamics and design optimasation of offshore energy wind conversation systems. Delft University of Technology, Delft, the Netherlands.

Le, C.H., Ding, H.Y., Zhang, P.Y., 2018. Prototype testing for the partial removal and repenetration of the mooring dolphin platform with multi-bucket foundations. Mar. Struct 59, 80–93.

Lian, J., Chen, F., Wang, H., 2014. Laboratory tests on soil-skirt interaction and penetration resistance of suction caissons during installation in sand. Ocean Eng. 84, 1–13.

Mehravar, M., Harireche, O., Faramarzi, A., 2016. Evaluation of undrained failure envelopes of caisson foundations under combined loading. Appl. Ocean Res. 59, 129–137.
Mehravar, M., Harireche, O., Faramarzi, A., Alani, A.M., 2017. Modelling the variation of suction pressure during caisson installation in sand using Flac3D. Ships and Offshore Structurs 12, 893–899.
Peck, R.B., Hanson, E.E., Thornburn, T.H., 1974. Foundation Engineering, 2nd ed. John Wiley and Sons, New York.
Senders, M., Randolph, M.F., 2009. CPT-based method for teh installation of suction caissons in sand. J. Geotech. Geoenviron. Eng. ASCE 14–25.
Senpere, D. & Auvergne, G. A., 1982. *Suction anchor piles- a proven alternative to driving or drilling.* Houston, Texas , In: Offshore Technology Conference (OTC4206).
Tjelta, T. I., Guttormsen, T. R. & Hermstad, J. 1986 Large-scale penetration test at a deepwater site s.l., In: Offshore Technology Conference Houston, TX, Paper OTC 5103.
Tjelta, T.I. Geotechnical aspects of bucket foundations replacing piles for the Europipe 16/11-E Paper OTC 7379, In: Offshore Technology Conference (OTC) 1994 Houston, Texas.
Tjelta, T. I., 1995. *Geotechnical experience from the installation of the Europipe jacket with bucket foundations.* Houston, Texas, Paper OTC 7795, In: Offshore Technology Conference .
Tran, M. N., Randolph, M. F. & Airey, D. W., 2004. *Experimental study of suction installation of caissons in dense sand.* Vancouver, Canada , In: proceedings of the 23rd International Conference on Offshore Mechanics and Arctic Engineering .
Tran, M. N., Randolph, M. F. & Airey, D. W., 2005. *Study of seepage flow and sand plug loosening in installation of suction caissons in sand.* Seoul, South Korea , In: 15th International Offshore and Polar Engineering Conference.
Tran, M.N., Randolph, M.F.A.D.W., 2007. Installation of suction caisson in sand with silt layers. J. Geotech. Geoenviron. Eng. 133 (10), 1183–1191.
Tran, M.N., Randolph, M.F., 2008. Variation of suction pressure during caisson installation in sand. Geotechnique 58 (11), 1–11.
Vasquez, L.F., Tassoulas, J.L., 2000. Finite element analysis of suction piles. European Congress on Computational Methods in Applied Sceince and Engineering, Barcelona, In.
Vilalobos, F. A., Houlsby, G. T. & Byrne, B. W., 2004. *Suction caisson foundations for* offshore *wind turbines.* Santiago , Proc. 5th Chilean Conference of Geotechnics.
Villalobos, F. A., 2006. *Model testing of foundations for offshore wind turbines. PhD Dissertation ,* Oxford, UK : University of Oxford . Villalobos, F. a., Houlsby, G. T. & Byrne, B. W., 2004. *Suction caisson foundations for offshore wind turbines.* Santiago, Proc. 5th Chilean Conference of Geotechnics (Congreso Chileno de Geotecnia), pp. 24-26.
Wang, X., et al., 2018. A review on recent advancement of substructure for offshore wind turbines. Energ. Conver. Manage. 103–119.
Wang, Q., Zhou, X., Zhou, M., Tian, Y., 2020. Investigation on the behavior of stiffened caisson installation in uniform clay from large deformation modeling. Int. J. Geomech. 20 (9), 04020149.
Wang, Q., Zhou, X., Zhou, M., Hu, Y., 2021. Inner soil heave of stiffened caisson during installation in soft-over-stiff clay. Comput. Geotech. 138, 104336.
Wu, Y., Li, D., Zhang, Y., Chen, F., 2017. Determination of maximum penetration depth of suction caissons in sand. KSCE J. Civil Eng. 22 (1), 2776–2783.
Zhang, P., et al., 2017. Comparative analysis of seepage field charachteristics in bucket foundation with and without compartments. Ocean Eng. 143, 34–49.
Zhang, P., et al., 2018. Effect of seepage on the penetration resistance of bucket foundations with bulkheads for offshore wind turbines in sand. Ocean Eng. 156, 82–92.
Zhang, P., Zhang, Z., Liu, Y., Ding, H., 2016. Experimental study on installation of composite bucket foundations for offshore wind turbines in silty sand. J. Offshore Mechanics and Arctic Eng. 138.
Zhao, l., et al., 2018. Drained capacity of a suction caison in sand under inclined loading. J. Goetechn. Gooenviron. Eng. 145.
Zhou, M., Hossain, M.S., Hu, Y., Liu, H., 2016. Installation of stiffened caissons in nonhomogeneous clays. J. Geotech. Geoenviron. Eng. 142 (2), 04015079.
Zhou, M., Han, Y., Zhang, X., Ding, X., 2022. The scale effect on the failure mechanism and penetration resistance of caisson piling in clay. Acta Geotech. 1–14.
Zhu, B., Zhang, W.L., Ying, P.P., Chen, Y.M., 2014. Deflection-based bearing capacity of suction caisson foundations of offshore wind turbines. J. Geotech. Geoenviron. Eng. 140.